Research Article | Vol. 27, No. 8 | 15 Apr 2019 | OPTICS EXPRESS 11492
Optics EXPRESS

Voltage-controlled formation of short pitch chiral liquid crystal structures based on high-resolution surface topography

INGE NYS,* JEROEN BEECKMAN, AND KRISTIAAN NEYTS

LCP Group, ELIS Department, Ghent University, Technologiepark-Zwijnaarde 126, 9052 Gent, Belgium
*inge.nys@ugent.be

Abstract: Chiral nematic liquid crystals (CLCs) offer interesting perspectives for device applications and are fascinating materials to study because of their ability to self-assemble into complex structures. This work demonstrates that narrow lines of electron-beam resist on top of an ITO coated glass surface can dramatically influence the formation and growth of short pitch chiral superstructures in the bulk. By applying a voltage to the cell, directional growth of CLC structures along the corrugated surface can be controlled. Below the electric unwinding threshold, chiral structures start to grow along the grating lines with their helical axis parallel to the substrates. This results in a uniform lying helix-like structure at intermediate voltages and a chiral configuration with periodic undulations of the helical axis at low voltages.

1. Introduction

Electro-optic devices that modulate the properties of light have become indispensable in our daily lives since they are the enabling components in displays, cameras, lasers, LEDs, etc. Liquid crystals (LCs) are organic soft materials that are often used in electro-optic devices since they combine anisotropic optical properties with strong responsiveness to electric fields. LCs are nowadays widely used in flat panel displays, known as liquid crystal displays (LCDs), but they can also be used in many other photonic and non-photonic applications [1–5]. LCs combine fluidic properties of a liquid with a certain degree of long range ordering of the constituent mesogens. The average orientation of the molecular long-axis in the nematic liquid crystal (NLC) phase is called the director. In chiral nematic liquid crystal (CLC) the constituent mesogens are chiral, leading to a periodic rotation of the director over a macroscopic length scale. The CLC director describes a helical structure in space and the spatial period over which the director rotates over 2π is called the pitch p. The self-organization of CLC in a helical superstructure gives rise to material properties that are unachievable with achiral LC, such as the existence of a selective reflection band for light with circular polarization corresponding to the handedness of the CLC [6]. This makes especially short pitch CLC, with a reflection band in the visible wavelength range, very interesting for application in tunable lasers, reflective displays, diffraction gratings, etc.

To develop functional LC devices it is essential to have control over the self-organization of the LC in the bulk. The LC director configuration in a confined geometry depends on a delicate balance between surface anchoring, elastic energy and, if an electric field is applied, dielectric energy. Not only the device geometry, the electrode configuration and the applied voltage, but also the (elastic) material properties and the degree of chirality of the LC mixture influence the resulting director configuration. Due to the interplay of parameters, patterning of the LC anchoring at the confining surfaces offers an easy and effective way to control the director configuration in the bulk. Besides mechanical rubbing and oblique evaporation, two other techniques that are commonly used are photo-alignment and surface topography [7].

#360287 https://doi.org/10.1364/OE.27.011492
Journal © 2019 Received 19 Feb 2019; revised 29 Mar 2019; accepted 29 Mar 2019; published 10 Apr 2019

Optics EXPRESS

These alignment techniques have the advantage that complex patterns in the alignment orientation can be easily achieved.

Photo-alignment makes use of (polarized) illumination to obtain a preferential LC orientation. Different illumination techniques (direct write, holography, plasmonic patterning) were optimized in recent years to obtain high-resolution, high-throughput and repeatable patterns with a low cost [8–14]. Photo-alignment is a very versatile method, but the spatial resolution is limited and the period of the alignment pattern should be above several hundred nanometer. There is still interest in other patterning techniques that can offer higher resolution or new possibilities.

Surface topography has been studied as a tool for the alignment of especially NLC. Surface structures were made by nano-imprint lithography, soft embossing, replica moulding, laser scanning lithography, ion beam milling, nanosphere lithography and e-beam lithography [15–24]. Berreman explained that NLC molecules preferentially align parallel to the groove direction of a surface grating and not perpendicular to it [25]. In this way the effect of the short periodic (~a few hundred nanometer) surface structures is averaged out to determine the orientation of the nematic director over a much larger length scale. A surface structure with parallel grating lines typically acts as a uniformly rubbed substrate for NLC.

More recently, the influence of surface topography on the alignment of CLC has also been investigated [18,19]. The behavior is much more complex because the grooves may have similar dimensions as the pitch of the CLC and the simple theory of Berreman does not apply anymore. In this case, besides the surface topography and surface chemistry, also the chiral pitch and the cell thickness strongly define the resulting director configuration. Previously Outram et al. exploited surface topography for CLC alignment by creating a mold-templated surface to align a short pitch (p = 320 nm) uniform lying helix (ULH) [18]. The channel width and height was much larger than the chiral pitch in this case. Carbone et al. used a surface produced by two-photon excitation laser-lithography to break the azimuthal degeneracy of the homeotropic alignment layer and roughly align a long pitch (p = 4 μm) ULH [19]. In these cases, the entire surface structure consisted of a single material and the effect on the CLC alignment was solely related to the surface topography.

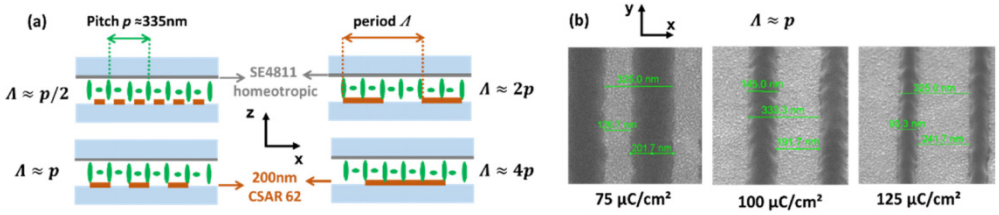

Fig. 1. (a) Schematic overview of the cell configuration and the four different grating periods Λ tested for the alignment of short pitch CLC (p ≈335 nm). The e-beam resist at the bottom substrate is removed in the exposed areas, resulting in isolated grating lines (along y) in which the LC is in contact with the ITO covered glass substrates [23]. (b) SEM images for the resulting e-beam resist lines (smooth dark lines) on top of an ITO-covered glass substrate (rough bright lines) after development for three different exposure doses (75 μC/cm^2, 100 μC/cm^2 and 125 μC/cm^2 from left to right) and grating period $\Lambda = p$.

In this work, a periodic surface structure at one of the confining glass substrates is created by e-beam lithography and its effect on the alignment and stabilization of short pitch (p ≈335 nm) helical structures in the bulk of the cell is investigated. The surface structure, consisting of alternating stripes with and without e-beam resist on the substrate, serves as a command layer for directional growth of CLC structures, that is controlled by applying a voltage to the cell. The e-beam lithography is performed on ITO-covered glass substrates and after development of the resist, a cell is produced in which the bottom substrate is covered by the patterned resist (Fig. 1(a)). Unlike in previous work [18], the dimensions of the surface structure are similar to the chiral pitch (335 nm). When the voltage is decreased below the

Optics EXPRESS

electric unwinding threshold, cholesteric fingers start growing along the surface grating. The behavior as a function of the voltage is studied in detail, also for lower voltages. This work is similar to the study of voltage controlled directional growth of long-pitch ($p \approx 4.6$ µm) material [23], but now short pitch ($p \approx 335$ nm) chiral structures are realized in cells with a larger thickness to pitch ratio. The much shorter chiral pitch used here requires much shorter dimensions for the period Λ of the grating pattern.

In contrast to previous work described in literature, our alignment technique for CLC gives rise to a ~200 nm pattern in which the LC is periodically in contact with two different materials (e-beam resist and ITO-coated glass). The surface chemistry of both materials is different and this gives rise to periodically varying anchoring: homeotropic above the ITO stripes and planar degenerate above the e-beam resist stripes [23]. This approach is similar to that of Li et al. who developed an e-beam lithography technique to obtain patterned substrates with alternating planar and homeotropic regions on a silicone substrate [26,27]. This technique requires more processing steps than our method and results in a flat patterned surface without topographic steps.

2. Sample preparation

To produce a LC cell, one lithographically patterned substrate is glued together with a flat ITO-covered glass substrate (Delta Technologies, ITO-coated float glass 1.1 mm), using glue (NOA68) that contains spherical spacer balls to define the spacing. The production process is schematically illustrated in Fig. 1. A mixture of NLC E7 (94.6 wt%) with positive dielectric anisotropy ($\varepsilon_\perp = 5.2$, $\varepsilon_\parallel = 19$) and chiral dopant BDH 1305 (5.4 wt%) is infiltrated in the cells. The cells are filled above the isotropic-chiral nematic transition temperature and cooled down slowly to room temperature. The analysis of the sample is done at room temperature. The pitch of the mixture is $p \approx 335$ nm and the cell gap is $d = 3.0$ µm for the experiments reported in section 3.1, and $d = 2.1$ µm for the experiments in section 3.2. To achieve electrical tuning, a sinusoidal potential difference with a frequency of 1 kHz is applied over the two uniform ITO electrodes of the top and bottom substrates. The reported values for the voltages are peak values V_p (not the root mean square values) of the potential difference.

The flat ITO-covered substrate is first treated with UV-ozone (15 min at 90°C, Novascan) and covered with a homeotropic alignment layer (SE4811, Nissan Chemical Industries). The production parameters are: spin speed 2500 rpm, spin time 15 s, tempering 2 min at 90°C on a hot plate and baking for 1 h at 180°C in the oven.

To obtain a lithographically patterned substrate, a ~200 nm layer of positive e-beam resist AR-P 6200.09 (CSAR 62) is spin-coated on top of an ITO-covered glass substrate (Delta Technologies, ITO coated float glass 1.1 mm) at 4000 rpm for 60 s. The layer is tempered at 150°C for 1 min on a hot plate and the resist is selectively exposed with an electron-beam using the VOYAGER e-beam system (Raith). The low-current mode with 60 µm aperture is used and results for different exposure doses (75 µC/cm^2, 90 µC/cm^2, 100 µC/cm^2 and 125 µC/cm^2) are reported, resulting in different fill-factors of the grating. After exposure by the e-beam, the resist is developed during 1 min in n-amyl acetate and for stopping the development the sample is submerged during 30 s in IPA and 30 s in DI water. The e-beam resist is removed in the exposed grating lines but remains present on top of the substrate in the non-exposed areas.

Four different ratios between the pitch and the surface grating structure are tested (Fig. 1). The smallest period is $\Lambda \approx p/2 = 168$ nm (resulting in grating lines that are less than 100 nm wide). The width of the remaining e-beam resist stripes after development was a bit larger than $\Lambda/2$ for exposure dose 75 µC/cm^2 and a bit smaller than $\Lambda/2$ for higher doses (100 µC/cm^2 and 125 µC/cm^2). This is illustrated in the Fig. 1(b) for the grating with $\Lambda \approx p$. An optimized dose of 90 µC/cm^2 was used for the 2.1 µm thick sample reported in section 3.2 (SEM image not shown).

Optics EXPRESS

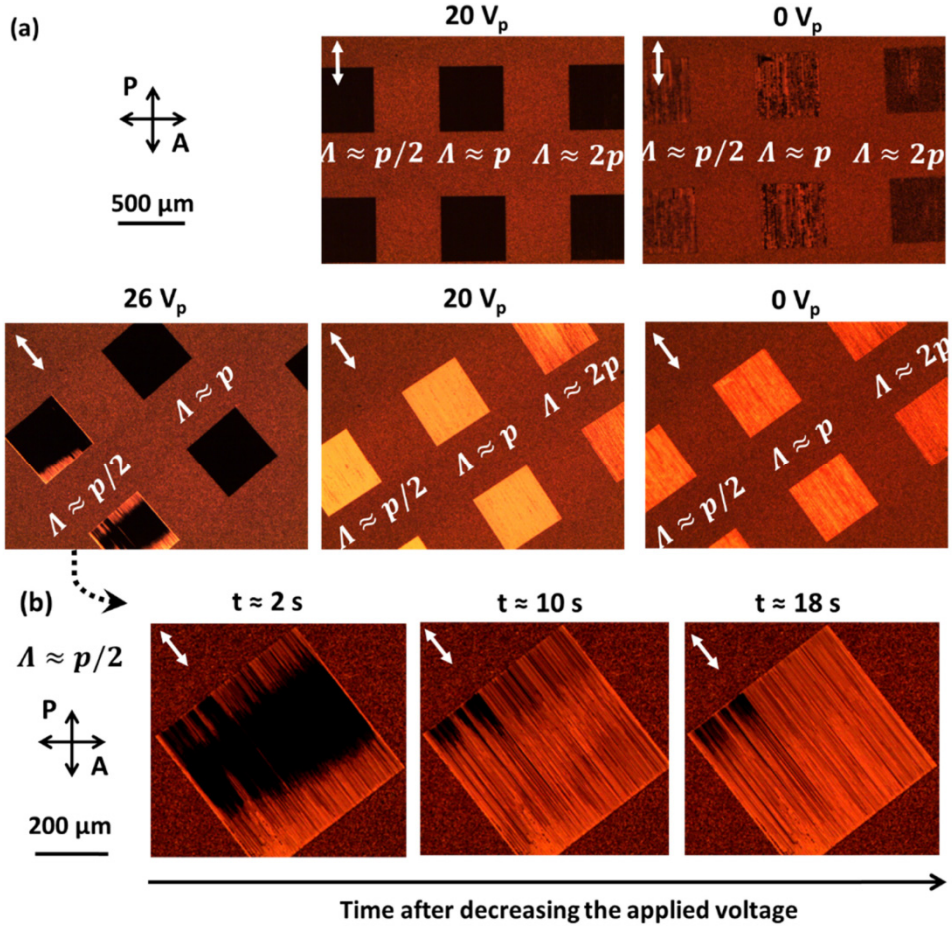

Fig. 2. (a) POM images for decreasing voltages (26 V_p, 20 V_p and 0 V_p), with the grating rotated over 0° (top) and ± 37° (bottom) with respect to the crossed polarizers. (b) POM images (for the grating with $\Lambda = p/2$) for different time intervals after decreasing the voltage to 26 V_p. The orientation of the grating lines is indicated by the white arrow. The cell thickness is d = 3.0 µm, the pitch p = 335 nm and the illumination dose of the grating was 75 µC/cm^2. Outside the square grating areas, resist is still present on top of the ITO-covered glass substrate.

3. Experimental results

3.1 Experimental results in a 3 µm thick cell

At high applied voltages, the LC is aligned vertically in the bulk, resulting in a dark image in polarizing optical microscopy (POM). A relatively large voltage (~30 V_p) is necessary to align the LC vertically in the bulk since the electric unwinding threshold is inversely proportional to the chiral pitch [28,29]. The critical field for dielectric unwinding E_c of CLC was derived by Kahn [28]:

$$E_C = \frac{\pi^2}{p}\sqrt{\frac{K_{22}}{\varepsilon_0 \Delta\varepsilon}} \qquad (1)$$

with p the chiral pitch, K_{22} the twist elastic constant and $\Delta\varepsilon$ the dielectric anisotropy (at electrical frequencies). Patel and Meyer slightly adjusted this formula by taking into account the flexoelectric contribution [29]. Using Eq. (1) we can estimate that the critical field for

Optics EXPRESS

dielectric unwinding in our material (p = 335 nm, K_{22} = 6.5 pN, $\epsilon_{\perp}$ = 5.2 and $\epsilon_{\parallel}$ = 19.0) is approximately $E_c \approx$6.8 V/µm. This corresponds to a voltage of $V_{rms} \approx$20.4 V, corresponding to ≈29 V_p in our 3 µm thick cell and is in good quantitative agreement with the experimentally observed values.

When the voltage is decreased to ~28 Vp, a randomly oriented focal conic structure appears in the unpatterned regions (where the bottom substrate is covered with resist), while vertical alignment is conserved in the patterned area. A small further reduction of the voltage leads to directional growth of bright cholesteric fingers parallel to the e-beam resist lines (Fig. 2), starting from the grating edges. The onset voltage for the growth is slightly different for the different periods ($\Lambda \approx p/2$, p, 2p or 4p) and is the highest (1 Vp higher than for the others) for the gratings with $\Lambda \approx p/2$ (Fig. 2(a)). It is not completely clear if this is due to the change in surface period or if other effects play a role (for example the local cell thickness, or the fill factor of the grating).

The growth of the bright cholesteric fingers after decreasing the voltage is shown in more detail in Fig. 2(b). An increasing number of cholesteric fingers start to grow and fill the grating area, after the voltage is decreased below the threshold voltage. When the grating is oriented at 45° with respect to the crossed polarizers, the brightness increases with time, while the transmission remains low when the grating is aligned along one of the polarizers (Fig. 2(a)).

When the voltage is decreased further in small steps, the transmission for the grating orientation at ± 45° between crossed polarizers reaches a maximum at an intermediate voltage (~20 V_p) and then decreases (Fig. 2(a) and Fig. 3). The degradation of the optical properties upon reduction of the voltage is also visible when the grating lines are oriented parallel to one of the polarizers, as an increased light leakage at low voltages (Fig. 2(a) and Fig. 3).

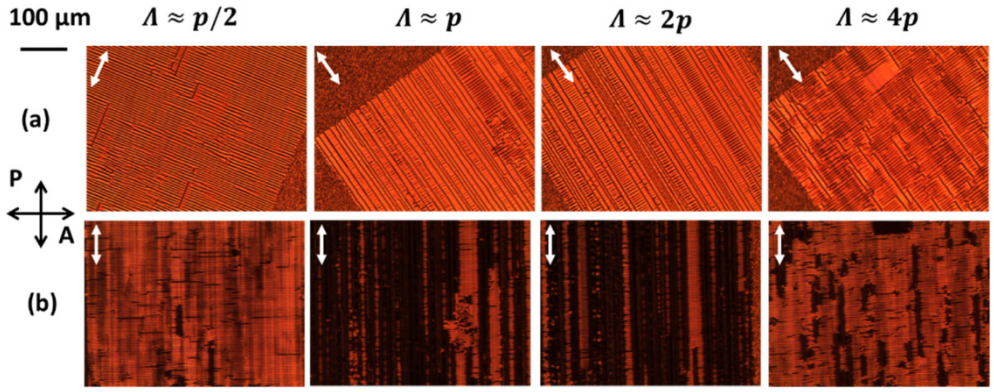

Fig. 3. POM images at 0 V with the grating lines under an angle of 35° with the crossed polarizers (a) and with the grating lines aligned with the analyzer (b). The orientation of the grating lines is indicated with a white arrow. The cell thickness is 3.0 µm, the pitch p = 335 nm and the illumination dose was 75 µC/cm^2. Four different ratios between Λ and p are shown.

When we look into more detail at the POM images at low voltages (below ~10 V_p), we observe perturbations in the structure (Fig. 3 and Fig. 4). The nature of these perturbations depends on the Λ/p ratio and on the fill-factor of the grating (due to different exposure doses), but in all cases a periodicity perpendicular to the grating lines (along y) is developed. For $\Lambda \approx p$ and $\Lambda \approx 2p$ in Fig. 3 this periodicity is only maintained in small regions and is interrupted by defects parallel to the grating lines. For $\Lambda \approx p/2$ and $\Lambda \approx 4p$ a pronounced periodicity perpendicular to the grating lines is observed over large areas, with few defect lines.

Figure 4. focuses in more detail on the periodicity perpendicular to the grating lines that is developed at low voltages. Results are shown for the grating with the smallest period ($\Lambda \approx p/2$) for decreasing voltages. It is clear that the perturbations become more pronounced and the

Optics EXPRESS

period increases when the voltage is lowered: at 6 V_p the period is about 2.5 µm, at 0 V_p the period is about 5 µm. A similar behavior is seen for gratings with a different fill-factor.

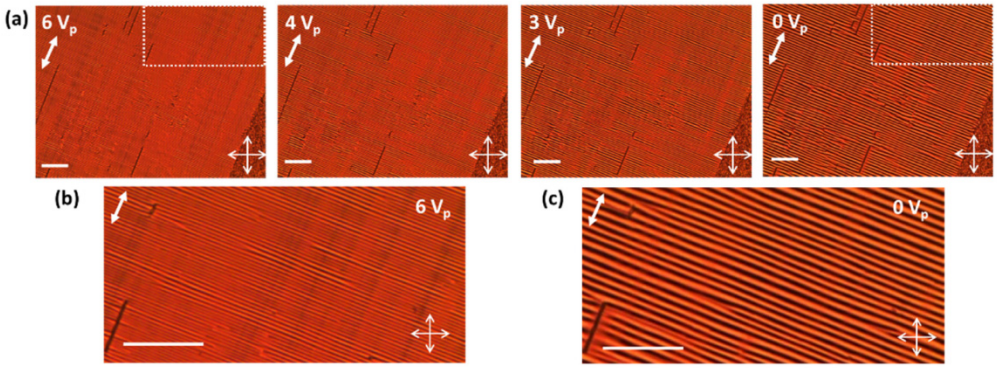

Fig. 4. (a) POM images at 6 V_p, 4 V_p, 3 V_p and 0 V_p with the grating lines under an angle of 23° with the crossed polarizers. (b,c) Enlarged image at 6 V_p (b) and 0 V_p (c). The orientation of the grating lines is indicated with a white arrow. The scale bar in all images has a length of 50 µm. The cell thickness is 3.0 µm, the pitch p = 335 nm and the illumination dose was 75 µC/cm^2. The periodicity of the grating lines is $\Lambda \approx p/2$.

3.2 Experimental results in a 2.1 µm thick cell

In a thinner cell with thickness d = 2.1 µm instead of 3.0 µm, similar results are obtained as summarized in Fig. 5. Directional growth of bright cholesteric structures along the grating lines is observed at high voltages (after reducing V_p just below the unwinding threshold) and a periodicity perpendicular to the grating lines is developed at lower voltages.

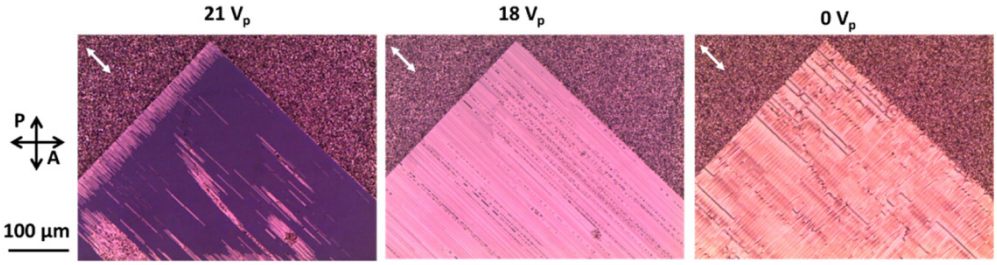

Fig. 5. POM images at 21 V_p, 18 V_p and 0 V_p with the grating lines under an angle of 45° with the crossed polarizers. The orientation of the grating lines is indicated with a white arrow. The cell thickness is 2.1 µm, the pitch p = 335 nm and the illumination dose was 90 µC/cm^2. The periodicity of the grating lines is $\Lambda = p/2$.

Only subtle differences are present between the behavior in the 2.1 and 3 µm thick cell. In the thinner cell, defects nucleate more easily when the voltage is decreased. These defects, when present in the grating area, serve as starting points for the growth of cholesteric fingers inside the grating area. Therefore, in the 2.1 µm thick cell the growth of cholesteric fingers frequently starts at defects inside the grating area (Fig. 5, left) while in the 3 µm thick cell the cholesteric stripes predominantly start growing from the grating edges (Fig. 2). The smaller cell thickness and lower retardation also results in different colors of the cholesteric structure.

4. Discussion

When the voltage is decreased from a high value, we observe the directional growth of cholesteric fingers along the grating lines. The homeotropic unwound regions disappear and more cholesteric fingers appear at lower voltages. This can be explained by the reduced importance of electric energy with respect to elastic energy at lower voltages. In these short

Optics EXPRESS

pitch CLC samples, at intermediate voltages (~20 V_p) the average transmission is very low when the grating is aligned with one of the polarizers. This indicates that the director is everywhere more or less parallel to the yz-plane and that the cholesteric structure has its helical axis parallel to the x-axis (as defined in Fig. 1).

At lower voltages, perturbations of the cholesteric structure along the grating lines are observed. Figures 3-5 show more or less parallel bright and dark bands (along x) perpendicular to the grating lines (along y). The director configuration is periodically modulated with a period and amplitude that depends on the voltage. These perturbations of the structure at small voltages can be explained by undulations of the helical axis in the xy-plane. Such undulations lead to periodic changes of the transmission along the y-axis, when observed between crossed polarizers (Fig. 6). Due to these undulations the average transmission is lower than expected when the grating is oriented at 45° between crossed polarizers, and higher when the grating is oriented at 0° (Figs. 2-5).

Undulations of the helical axis would not appear if the grating area were completely filled with a ULH structure that matched the pitch of the CLC. In our experiments we start at high voltages, with the CLC completely unwound, resulting in a uniform homeotropic director. By lowering the voltage, more and more cholesteric fingers are added in the grating area by growth from the border region. However, we can expect that the energy threshold to generate an additional cholesteric finger prevents that the ULH fully develops with the same periodicity as the intrinsic pitch *p* of the material. As a result the distance between neighboring cholesteric fingers (in the x-direction) remains larger than the distance preferred by the intrinsic pitch. It is however possible to reduce the effective pitch (and the elastic energy) of the cholesteric structure by allowing the helical axis to tilt away from the x-axis. We believe that this effect may explain the observed undulations in the POM images. The cholesteric structures are anchored on the straight photolithographic lines at the bottom substrate, but are free to undulate in the bulk and at the top substrate. For decreasing voltages, the electric torque decreases and the structures have more freedom to undulate.

To get better insight in the undulation behavior of the helical axis we performed a numerical simulation. The finite element Q-tensor approach was used to find the director configuration in the bulk and the Jones Calculus was applied to simulate the transmission between crossed polarizers. The Q-tensor simulation tool has been developed at UCL and makes use of a minimization of the Landau-de Gennes free energy functional to find the spatial distribution of the LC director in the device [30–33]. The electrostatic field is determined from the variational form of Laplace's equation. In our simulations, the elastic and dielectric properties of E7 are used (K_{11} = 11.1 pN, K_{22} = 6.5 pN, K_{33} = 17.1 pN, $\epsilon_\perp$ = 5.2 and $\epsilon_\parallel$ = 19.0) After simulating the director distribution, the transmission between crossed polarizers is found by using Jones Calculus. The azimuth and inclination of the director are calculated on a regular grid and the transmission for light propagating along the z-axis is simulated as a function of the x- and y-coordinate. Jones Calculus is performed for three different wavelengths (430 nm, 530nm and 630 nm) and the results are combined to find the average transmitted intensity between crossed polarizers. The refractive indices of the LC E7 that are used in the simulations are n_o = 1.52 and n_e = 1.74.

We performed simulations for a simplified device geometry and for an applied voltage of 6 V_p as used in Fig. 4(b). The cell thickness (3 μm) and chiral pitch (335 nm) are the same as in the experiment. Periodic boundary conditions are used, with period 0.7 μm in the x-direction (corresponding to approximately twice the intrinsic pitch *p*) and 2.5 μm in the y-direction (corresponding to the period in Fig. 4(b) at 6 V_p). The periodicity along the x-direction is chosen to represent a situation with approximately half of the grating filled with cholesteric fingers. For simplicity, the surface topography is not taken into account and the anchoring of the cholesteric structure is fixed at the bottom substrate. At the bottom substrate, the director makes a 2π rotation over 335 nm and remains homeotropic in the rest of the interval (Fig. 6(c)). At the top substrate the director is left free, with zero torque. This is

Optics EXPRESS

different from the homeotropic anchoring in the experiment but considerably simplifies the simulation task [23], without strongly influencing the undulation behavior in the bulk.

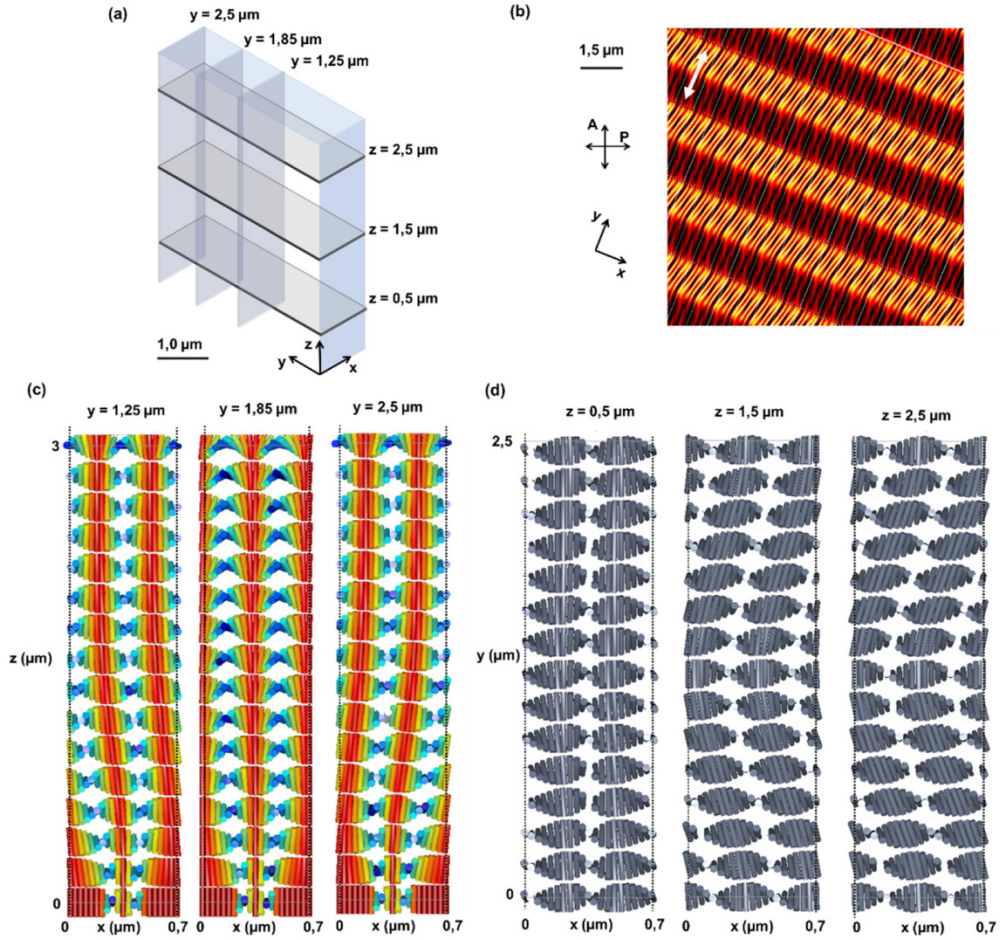

Fig. 6. Simulation results for the director configuration (c,d) and the transmission between crossed polarizers (b) for a short pitch (p = 335 nm) CLC structure with undulations of the helical axis at 6 V_p. (a) Overview of the simulated domain with dimensions 0.7 µm x 2.5 µm x 3.0 µm, with indication of the cross sections used in (c) and (d). Periodic boundary conditions are used in the x- and y-direction, while the anchoring is fixed at the bottom substrate and left free at the top substrate. (b) The transmission is simulated for an orientation of the grating lines (white arrow) of 22.5° between crossed polarizers, as for the experiments in Fig. 4.

The simulation results in Fig. 6 clearly indicate that an undulating structure appears when the grating is not completely filled with a cholesteric structure that matches the pitch of the CLC. The helical axis tilts out of the xy-plane close to the bottom substrate and forms an in-plane undulation pattern (variation of the helical axis in the xy-plane) in the bulk (Fig. 6). The amplitude of the in-plane undulation increases away from the bottom substrate, as can be seen in Fig. 6(d). The fact that an in-plane undulation of the helical axis (rather than an out-of-plane tilt) is preferred in the upper part of the cell, is related to the minimization of the electric energy when a voltage is applied (6 V_p). From Fig. 6(b) it is clear that this type of director configuration can explain the experimentally observed POM images in Fig. 4. The Jones Calculus does not take into account diffraction and the reproduction of submicrometer features in the image (Fig. 6(b)) is unreliable, but the periodic bright and dark bands in the POM images are well reproduced.

Optics EXPRESS

In general, the experiments show that the periodic surface structure strongly influences the formation of short pitch chiral structures in the bulk of the cell. The surface periodicity ($\Lambda \approx p/2$, p, $2p$ or $4p$) and the fill-factor of the grating turn out to be of minor importance for the overall behavior. The grating lines help the cholesteric structures to nucleate and grow along a certain direction and the dimension of the lines is not so important since the contribution of the surface energy is small with respect to the bulk elastic energy. Only for the highest e-beam dose of 125 μC/cm^2 and the smallest grating period $\Lambda \approx p/2$ the experiments failed. In this case the e-beam resist was overexposed and only small unconnected dots of resist were left on the substrate after development. After filling the cell, air bubbles were present on top of this area and no directional growth of CLC structures was observed.

Although the dimensions are completely different, several similarities are observed between the behavior for the short pitch samples (p = 335 nm, d = 2.1 or 3.0 μm) reported here and the long-pitch CLC samples (p = 4.6 μm, d = 12 μm) in previous work [23]. In the current experiments the chirality of the material is much stronger and the d/p ratio is larger. Therefore, a stronger influence of bulk elastic energy can be expected, while in the long-pitch CLC samples the transition from the surface to the bulk structure had a strong influence on the total free energy. When Λ was halved or doubled with respect to p in the long pitch experiments, the mismatch between the cholesteric structure in the bulk and the anchoring at the surface resulted in uncontrolled growth of cholesteric structures [23]. The fact that the short pitch CLC samples are less sensitive to this and show well-directed growth for $\Lambda \approx p/2$, p, $2p$ and $4p$, seems related to the larger d/p ratio but also the larger h/d and h/p ratio, with h the height of the grating structure. A larger surface topography might improve the anchoring of the cholesteric stripes to the grating lines, reducing the tendency for the cholesteric structures to grow in random directions as observed in [23].

Finally, we should remark that all these results only hold for a stepwise decrease of the voltage with a limited voltage difference between subsequent steps. When the voltage is decreased in large steps (~2 V_p per step or more), uncontrolled growth of a lying helix-like structure is observed experimentally, with a large amount of defects. This is also the case when the voltage is removed from a value close to the unwinding threshold (e.g. 30 V_p immediately to 0 V_p in the 3 μm thick cell). Cholesteric fingers are no longer growing along the grating lines, but the whole area is immediately filled with a cholesteric structure. The grating lines induce an asymmetry in the surface anchoring and this induces some preferred orientation of the lying helix structure as demonstrated before [18,19,33]. In this work a more controlled growth of cholesteric structures with a decreased number of defects is demonstrated, by decreasing the voltage in small steps (~1 V_p per step).

5. Summary

Self-organization of chiral superstructures in CLC is a powerful tool in developing functional devices and the experimental results presented here clearly indicate that the chiral ordering in the bulk can be manipulated by surface topography. We show that a periodic e-beam resist structure at one of the confining substrates dramatically influences the alignment of CLC structures. The electric-field-induced growth of short pitch cholesteric structures along the grating lines has been studied. Directional growth of short pitch cholesteric fingers along the surface gratings is observed below the electric unwinding threshold. By decreasing the voltage in small steps, controlled growth is obtained in short pitch CLC samples with a large thickness-to-pitch ratio. Cholesteric fingers grow along the grating lines and similar behavior is observed for different surface periodicities ($\Lambda \approx p/2$, p, $2p$ or $4p$) and fill-factors of the grating. At intermediate voltages, a ULH-like structure is obtained with high-quality bright and a dark states at orientations of respectively 45° and 0° between crossed polarizers. The grating area does not contain enough cholesteric fingers to attain a ULH with the intrinsic pitch and undulation of the cholesteric axis was observed at lower voltages, leading to a

Optics EXPRESS

periodicity perpendicular to the grating lines. We could unravel the nature of these undulations by numerical simulation of the director configuration.

In conclusion, enhanced control over the formation of chiral structures has been obtained with the help of an e-beam lithography structure at the surface. The straight-forward lithography technique has the advantage that small scale structures with different complex shapes are easily achievable and that the effect of surface topography can be combined with periodically modulated surface chemistry. Moreover, this versatile method for patterning the LC anchoring may be combined with appropriately patterned electrodes. This approach could be further exploited in the future by using different cell thicknesses, different thicknesses of the resist layer and different patterned electrodes and could be very interesting for application in electro-optic devices such as diffraction gratings, lasers and displays. Short pitch ULH-like structures are especially interesting to develop in-plane emitting CLC lasers and displays based on fast flexoelectro-optic switching [18,34,35,36]. Depending on the lateral dimensions that are envisioned, e-beam lithography could also be replaced by conventional UV lithography.

Funding

Research Foundation - Flanders (FWO) (FWO14/ASP/177).

References

1. S. J. Woltman, G. D. Jay, and G. P. Crawford, "Liquid-crystal materials find a new order in biomedical applications," Nat. Mater. **6**(12), 929–938 (2007).
2. A. d'Alessandro, L. Martini, G. Gilardi, R. Beccherelli, and R. Asquini, "Polarization-independent nematic liquid crystal waveguides for optofluidic applications," IEEE Photonics Technol. Lett. **27**(16), 1709–1712 (2015).
3. J. P. F. Lagerwall and G. Scalia, "A new era for liquid crystal research: Applications of liquid crystals in soft matter nano-, bio- and microtechnology," Curr. Appl. Phys. **12**(6), 1387–1412 (2012).
4. J. Beeckman, K. Neyts, and P. J. M. Vanbrabant, "Liquid-crystal photonic applications," Opt. Eng. **50**(8), 081202 (2011).
5. Q. Li, *Liquid Crystals Beyond Displays: Chemistry, Physics, and Applications* (John Wiley & Sons, 2012). doi:10.1002/9781118259993
6. I. Dierking, "Chiral liquid crystals: structures, phases, effects," Symmetry (Basel) **6**(2), 444–472 (2014).
7. K. Takatoh, M. Sakamoto, R. Hasegawa, M. Koden, N. Itoh, and M. Hasegawa, *Alignment Technology and Applications of Liquid Crystal Devices* (CRC, 2005).
8. M. N. Miskiewicz and M. J. Escuti, "Direct-writing of complex liquid crystal patterns," Opt. Express **22**(10), 12691–12706 (2014).
9. J. Kim, Y. Li, M. N. Miskiewicz, C. Oh, M. W. Kudenov, and M. J. Escuti, "Fabrication of ideal geometric-phase holograms with arbitrary wavefronts," Optica **2**(11), 958–964 (2015).
10. Y. Guo, M. Jiang, C. Peng, K. Sun, O. Yaroshchuk, O. Lavrentovich, and Q.-H. Wei, "High-resolution and high-throughput plasmonic photopatterning of complex molecular orientations in liquid crystals," Adv. Mater. **28**(12), 2353–2358 (2016).
11. I. Nys, J. Beeckman, and K. Neyts, "Switchable 3D liquid crystal grating generated by periodic photo-alignment on both substrates," Soft Matter **11**(39), 7802–7808 (2015).
12. I. Nys, V. Nersesyan, J. Beeckman, and K. Neyts, "Complex liquid crystal superstructures induced by periodic photo-alignment at top and bottom substrates," Soft Matter **14**(33), 6892–6902 (2018).
13. K. Kawai, M. Sakamoto, K. Noda, T. Sasaki, N. Kawatsuki, and H. Ono, "Tunable dichroic polarization beam splitter created by one-step holographic photoalignment using four-beam polarization interferometry," J. Appl. Phys. **121**(1), 013102 (2017).
14. I. Nys, K. Chen, J. Beeckman, and K. Neyts, "Periodic planar-homeotropic anchoring realized by photoalignment for stabilization of chiral superstructures," Adv. Opt. Mater. **6**(6), 1701163 (2018).
15. H. Takahashi, T. Sakamoto, and H. Okada, "Liquid crystal device with 50 nm nanogroove structure fabricated by nanoimprint lithography," J. Appl. Phys. **108**(11), 113529 (2010).
16. H.-G. Park, J.-J. Lee, K.-Y. Dong, B.-Y. Oh, Y.-H. Kim, H.-Y. Jeong, B.-K. Ju, and D.-S. Seo, "Homeotropic alignment of liquid crystals on a nano-patterned polyimide surface using nanoimprint lithography," Soft Matter **7**(12), 5610–5614 (2011).
17. D. R. Chiou, L. J. Chen, and C. D. Lee, "Pretilt angle of liquid crystals and liquid-crystal alignment on microgrooved polyimide surfaces fabricated by soft embossing method," Langmuir **22**(22), 9403–9408 (2006).
18. B. I. Outram, S. J. Elston, R. Tuffin, S. Siemianowski, and B. Snow, "The use of mould-templated surface structures for high-quality uniform-lying-helix liquid-crystal alignment," J. Appl. Phys. **113**(21), 213111 (2013).

Optics EXPRESS

19. G. Carbone, D. Corbett, S. J. Elston, P. Raynes, A. Jesacher, R. Simmonds, and M. Booth, "Uniform lying helix alignment on periodic surface relief structure generated via laser scanning lithography," Mol. Cryst. Liq. Cryst. (Phila. Pa.) **544**(1), 37–49 (2011).
20. S. P. Palto, A. R. Geivandov, I. V. Kasyanova, V. V. Artemov, and M. V. Gorkunov, "Micro- and nanostructures for the spatially periodic orientation of liquid crystals obtained by focused ion beam milling," Condens. Matter **105**(3), 174–178 (2017).
21. M. Wahle, K. Brassat, J. Ebel, J. Bürger, J. K. N. Lindner, and H.-S. Kitzerow, "Two-dimensional switchable blue phase gratings manufactured by nanosphere lithography," Opt. Express **25**(19), 22608–22619 (2017).
22. T. Kagajyo, K. Fujibayashi, T. Shimamura, H. Okada, and H. Onnagawa, "Alignment of nematic liquid crystal molecules using nanometer-sized ultrafine patterns by electron beam exposure method," Jpn. J. Appl. Phys. **44**(1B), 578–581 (2005).
23. I. Nys, J. Beeckman, and K. Neyts, "Surface-mediated alignment of long pitch chiral nematic liquid crystal structures," Adv. Opt. Mater. **6**(13), 1800070 (2018).
24. I. V. Kasyanova, A. R. Geivandov, V. V. Artemov, M. V. Gorkunov, and S. P. Palto, "Nematic liquid crystal alignment on subwavelength metal gratings," Beilstein J. Nanotechnol. **9**, 42–47 (2018).
25. D. W. Berreman, "Alignment of liquid crystals by grooved surfaces," Mol. Cryst. Liq. Cryst. (Phila. Pa.) **23**(3–4), 215–231 (1973).
26. X. Li, J. C. Armas-Perez, J. A. Martinez-Gonzalez, X. Liu, H. Xie, C. Bishop, J. P. Hernandez-Ortiz, R. Zhang, J. J. de Pablo, and P. F. Nealey, "Directed self-assembly of nematic liquid crystals on chemically patterned surfaces: morphological states and transitions," Soft Matter **12**(41), 8595–8605 (2016).
27. J. A. Martínez-González, X. Li, M. Sadati, Y. Zhou, R. Zhang, P. F. Nealey, and J. J. de Pablo, "Directed self-assembly of liquid crystalline blue-phases into ideal single-crystals," Nat. Commun. **8**, 15854 (2017).
28. F. J. Kahn, "Electric-field-induced color changes and pitch dilation in cholesteric liquid crystals," Phys. Rev. Lett. **24**(5), 209–212 (1970).
29. J. S. Patel and R. B. Meyer, "Flexoelectric electro-optics of a cholesteric liquid crystal," Phys. Rev. Lett. **58**(15), 1538–1540 (1987).
30. R. James, E. Willman, F. A. FernandezFernandez, and S. E. Day, "Finite-element modeling of liquid-crystal hydrodynamics with a variable degree of order," IEEE Trans. Electron Dev. **53**(7), 1575–1582 (2006).
31. E. Willman, F. A. Fernández, R. James, and S. E. Day, "Modeling of weak anisotropic anchoring of nematic liquid crystals in the Landau-de Gennes theory," IEEE Trans. Electron Dev. **54**(10), 2630–2637 (2007).
32. E. Willman, F. A. Fernández, R. James, and S. E. Day, "Switching dynamics of a post-aligned bistable nematic liquid crystal device," J. Disp. Technol. **4**(3), 276–281 (2008).
33. R. James, F. Anibal Fernandez, S. E. Day, S. Bulja, D. Mirshekar-Syahkal, and M. Yazdanpanahi, "Finite Element Analysis of a Balanced Microstrip Line Filled with Nematic Liquid Crystal," in 2009 IEEE MTT-S International Microwave Symposium, **1–3**, (IEEE, 2009), pp. 133–136.
34. B. I. Outram and S. J. Elston, "Spontaneous and stable uniform lying helix liquid-crystal alignment," J. Appl. Phys. **113**(4), 043103 (2013).
35. C. C. Tartan, P. S. Salter, M. J. Booth, S. M. Morris, and S. J. Elston, "Localised polymer networks in chiral nematic liquid crystals for high speed photonic switching," J. Appl. Phys. **119**(18), 183106 (2016).
36. I. Nys, J. Beeckman, and K. Neyts, "One- and two-dimensional liquid crystal structures for lasing applications," Proc. SPIE **9565**, 956513 (2015).